

Scaling of Inhibitory Interneurons in Areas V1 and V2 of Anthropoid Primates as Revealed by Calcium-Binding Protein Immunohistochemistry

Chet C. Sherwood^a Mary Ann Raghanti^b Cheryl D. Stimpson^a
Christopher J. Bonar^c Alexandra A. de Sousa^a Todd M. Preuss^d Patrick R. Hof^{e, f}

^aDepartment of Anthropology, The George Washington University, Washington, D.C.,

^bDepartment of Anthropology and School of Biomedical Sciences, Kent State University, Kent, Ohio,

^cCleveland Metroparks Zoo, Cleveland, Ohio, ^dDivision of Neuroscience and Center for Behavioral Neuroscience, Yerkes National Primate Research Center, Emory University, Atlanta, Ga., ^eDepartment of Neuroscience, Mount Sinai School of Medicine, and ^fNew York Consortium in Evolutionary Primatology, New York, N.Y., USA

Key Words

Calbindin · Calretinin · Evolution · Parvalbumin · Visual cortex · Mammals · Primates

Abstract

Inhibitory GABAergic interneurons are important for shaping patterns of activity in neocortical networks. We examined the distributions of inhibitory interneuron subtypes in layer II/III of areas V1 and V2 in 18 genera of anthropoid primates including New World monkeys, Old World monkeys, and hominoids (apes and humans). Interneuron subtypes were identified by immunohistochemical staining for calbindin, calretinin, and parvalbumin and densities were quantified using the optical disector method. In both V1 and V2, calbindin-immunoreactive neuron density decreased disproportionately with decreasing total neuronal density. Thus, V1 and V2 of hominoids were occupied by a smaller percentage of calbindin-immunoreactive interneurons compared to monkeys who have greater overall neuronal densities. At the transition from V1 to V2 across all individuals, we found a tendency for increased percentages of calbindin-immunoreactive multipolar cells and calretinin-immunoreactive interneurons. In addition, parvalbumin-immunoreac-

tive cell soma volumes increased from V1 to V2. These findings suggest that modifications of specific aspects of inhibition might be critical to establishing the receptive field properties that distinguish visual areas. Furthermore, these results show that phylogenetic variation exists in the microcircuitry of visual cortex that could have general implications for sensory processing.

Copyright © 2007 S. Karger AG, Basel

Introduction

The histological organization of the mammalian cerebral cortex displays marked phylogenetic variation [Preuss, 2000; DeFelipe et al., 2002]. Populations of non-pyramidal inhibitory GABAergic interneurons, in particular, have been shown to differ in their somatodendritic geometry and distribution patterns among species [Hof et al., 1999; Hof and Sherwood, 2005]. The calcium-binding proteins, calbindin D-28k (CB), calretinin (CR), and parvalbumin (PV), are colocalized with GABA in morphologically and physiologically distinct non-overlapping subpopulations of interneurons [Andressen et al., 1993; DeFelipe, 1997]. In primates, it has been estimated

that 90–95% of all cortical GABAergic interneurons contain either CB, CR, or PV [Hendry et al., 1989; Van Bredere et al., 1990; Glezer et al., 1993; Carder et al., 1996]. In the primate cortex, most CR-immunoreactive (ir) interneurons resemble double-bouquet or bipolar cells. Although CB-ir neurons are more varied, they also include double-bouquet and bipolar neurons, as well as occasional large basket and chandelier cells [DeFelipe et al., 1999]. In contrast, the morphology of PV-ir interneurons in primates includes mostly large multipolar types, such as large basket and chandelier cells.

Given that interneurons are involved in fundamental aspects of intracortical processing [Tsumoto et al., 1979; Sato et al., 1995; Wang et al., 2000b], it is interesting that species differences exist in their proportional representation. For example, GABAergic cells constitute a greater percentage of all neurons in the macaque monkey medial prefrontal cortex (24.9%) than in the rat medial frontal cortex (16.2%) [Gabbott and Bacon, 1996; Gabbott et al., 1997a]. The distribution of specific types of calcium-binding protein-ir interneurons in the neocortex, moreover, shows distinct differences among major mammalian groups [Glezer et al., 1993; Hof et al., 1999]. Across the neocortex of cetaceans and artiodactyls, for instance, CB- and CR-ir interneurons predominate over PV-ir cells, whereas there is a more equal distribution among calcium-binding protein-ir subtypes in the neocortex of primates and rodents [Hof et al., 1999; Hof and Sherwood, 2005]. Scarce data exist, however, concerning more subtle differences in the distributions of cortical interneuron subtypes among closely related species. We recently reported that the proportions of different inhibitory interneurons in primary motor cortex varies among catarrhine primates [Sherwood et al., 2004]. We observed a greater percentage of PV-ir interneurons in great apes and humans relative to Old World monkeys, although there were no significant differences among these species in CB-ir and CR-ir neuron percentages. Although these results suggest that PV-ir interneurons have been selectively increased in the primary motor cortex of great apes and humans to subserve functional specialization, it is also possible that these changes relate to scaling effects that accompany the enlarged brain size of these species. At present, however, there are few comparative scaling analyses that address how different neurochemical systems change with variation in overall brain size [for an exception see Tower and Young, 1973]. Examination of the rules underlying chemoarchitectural allometry might provide an important insight into the computational design constraints that appear across scales of size. In addition, this gap in our cur-

rent understanding impedes progress in disentangling the predictable effects of scaling from deviations which might represent phylogenetic adaptations.

Here we examine calcium-binding protein-ir interneuron distributions in areas V1 and V2 across anthropoid primates (i.e., New World monkeys, Old World monkeys, and hominoids – apes and humans). One main goal of this study was to establish whether different scaling patterns exist for various interneuron subtypes and whether major phylogenetic groups of anthropoid primates diverge in these scaling relationships. A second aim of this study was to address whether V1 and V2 are distinguished by a common set of changes in the distribution of inhibitory interneurons across the major anthropoid groups.

Materials and Methods

Sample Preparation

Visual cortex samples from 27 adult individuals representing 18 anthropoid primate genera (19 species) were used in this study (table 1). Most specimens were donated by zoological or research institutions and were collected postmortem. These samples were fixed by immersion in 10% neutral buffered formalin after a postmortem delay of no more than 14 h. The remaining specimens were obtained from animals that were perfused transcardially with 4% paraformaldehyde in the context of unrelated experiments. Human brain specimens from two neurologically normal individuals were obtained from the Kathleen Price Bryan Brain Bank at Duke University Hospital. In all cases, brains were transferred to 0.1 M phosphate-buffered saline (PBS) containing 0.1% sodium azide and stored at 4°C after acquisition to mitigate excessive antigen blockage and tissue shrinkage.

Brain weights of nonhuman specimens were measured either immediately after perfusion or directly upon receipt from the donating institution. Human brain weights were measured at autopsy and were provided by the brain bank. Some artifact in our total brain weight data due to interindividual differences in fixation length was unavoidable. Nevertheless, shrinkage artifact is likely to be minimal because our brain weight measurements fall close to the normal range of values reported in the literature for fresh brains from these taxa [Stephan et al., 1981; Zilles and Rehkämper, 1988; Rilling and Insel, 1999].

Only the left hemisphere was used. Occipital lobe blocks were cryoprotected by immersion with increasing concentrations of sucrose solution up to 30%. Blocks were then frozen on dry ice and sections were cut at 30–50 µm using a sliding microtome and stored in separate numbered Eppendorf tubes in anatomical order. From each specimen, a 1:10 series of sections was stained for Nissl substance with a solution of 0.5% cresyl violet.

Immunohistochemical Staining

Immunohistochemistry was performed for each antigen on adjacent 1:20 series of sections. Free-floating sections were stained with monoclonal antibodies against PV (dilution 1:10,000) and

Table 1. The comparative sample used in this study

Species	Sex	Age	Fixation
<i>Homo sapiens</i>	F	73	I
<i>Homo sapiens</i>	M	72	I
<i>Pan troglodytes</i>	F	19	I
<i>Pan troglodytes</i>	M	41	I
<i>Gorilla gorilla</i>	F	50	I
<i>Gorilla gorilla</i>	M	13	I
<i>Pongo pygmaeus</i>	M	33	I
<i>Pongo pygmaeus</i>	M	11	I
<i>Hylobates muelleri</i>	M	19	I
<i>Papio anubis</i>	M	11	P
<i>Papio anubis</i>	M	11	P
<i>Mandrillus sphinx</i>	F	33	I
<i>Macaca maura</i>	F	7	P
<i>Macaca maura</i>	M	10	P
<i>Erythrocebus patas</i>	F	12	P
<i>Erythrocebus patas</i>	M	12	P
<i>Cercopithecus kanditi</i>	M	adult	I
<i>Colobus angolensis</i>	M	18	I
<i>Alouatta caraya</i>	M	21	I
<i>Ateles geoffroyi</i>	F	26	P
<i>Saimiri boliviensis</i>	F	12	P
<i>Saimiri sciureus</i>	F	12	P
<i>Aotus trivirgatus</i>	M	>18	P
<i>Saguinus oedipus</i>	F	6	I
<i>Leontopithecus rosalia</i>	F	11	I
<i>Leontopithecus rosalia</i>	M	6	I
<i>Pithecia pithecia</i>	F	1	I

I = Immersion; P = perfusion.

CB (dilution 1:8,000), or with a polyclonal antibody against CR (dilution 1:10,000; Swant, Bellinzona, Switzerland). Prior to immunostaining, sections were rinsed thoroughly in PBS, pretreated for antigen retrieval by incubation in 10 mM sodium citrate buffer (pH 3.5) at 37°C in an oven for 30 min, then immersed in a solution of 0.75% hydrogen peroxide in 75% methanol to eliminate endogenous peroxidase activity. Primary antibodies were diluted in a solution containing PBS with 2% normal serum and 0.1% Triton X-100 and incubated for approximately 48 h on a rotating table at 4°C. After rinsing in PBS, sections were incubated in the secondary antibody (either biotinylated anti-mouse IgG or biotinylated anti-rabbit IgG, dilution 1:200; Vector Laboratories, Burlingame, Calif., USA) and processed with the avidin-biotin-peroxidase method using a Vectastain ABC kit (Vector Laboratories). Immunoreactivity was visualized using 3,3'-diaminobenzidine (DAB) as a chromogen and intensified with nickel. For every specimen, specificity of the immunoreaction was confirmed by processing control sections as described above excluding the primary antibody. Immunostaining was completely absent in control sections. Because we were not able to obtain precise information concerning postmortem delay and length of time in fixation for many of the specimens in this sample, several cases had to be excluded due to poor immunohistochemical staining quality.

Only sections with clear staining of neuronal perikarya and dendrites were included in quantitative analyses. For each immunostained series, alternate sections were counterstained with cresyl violet to visualize non-immunoreactive neurons, cytoarchitectural boundaries, and cortical layers.

Identification of Cortical Areas and Interneuron Subtypes

Areas V1 and V2 were identified on the basis of their topological location and distinct appearance in materials stained for Nissl substance, CB, CR, and PV [Allman and McGuinness, 1988; Hof and Morrison, 1995; DeFelipe et al., 1999; Rosa and Krubitzer, 1999; Rosa et al., 2005]. The region of V1 used in this study was restricted to the opercular portion of the calcarine cortex towards the occipital pole. Area V2 was identified at the dorsal boundary between V1 and V2. The portion of V2 defined for stereologic sampling in the current study extended no more than 2 mm away from the termination of the V1/V2 border zone. This conservative distance for the extent of V2 was used because in smaller primate brains, such as the callitrichids (marmosets and tamarins), the cortex of V2 might only reach this far [Rosa et al., 1997]. In this way, we did not attempt to sample the full width of V2 in all species, given that the border adjoining V2 with higher-order visual cortical areas can be difficult to differentiate on the basis of cytoarchitecture [Hof and Morrison, 1995; Kaas, 2005].

All quantitative analyses were restricted to layers II/III because CB- and CR-ir interneurons predominate in superficial layers of the primate visual cortex [Morrison et al., 1998; Hof et al., 1999]. We used the nomenclature of Brodmann [1909] to designate cortical layers and sublayers. In V1, the elaboration of a stratified layer IV into multiple sublayers is present in all anthropoid primates [Allman and McGuinness, 1988], whereas a distinct upper layer IVA is absent in most strepsirrhines [Allman and McGuinness, 1988; Preuss and Kaas, 1996]. Thus, in the present study, layer IVA could be clearly identified in Nissl-stained sections from all species and this cytoarchitectural feature was used to demarcate the lower boundary of layer II/III used in stereologic sampling. In V2, the bottom of layer III was distinguished from layer IV as the transition from abundant large pyramidal cell somata to a band of dense small granular cells. It should be noted that according to an alternative interpretation of V1 lamination proposed by Hässler [1967], Brodmann's sublayers IVA and IVB are included in layer III. Therefore, under Hässler's terminology our stereological analyses within V1 included layer IIIa, but not layer IIIb or IIIc.

Total neuron density in layer II/III was used as a reference variable for analyses of interneuron subtype densities. We quantified total neuron density from Nissl-stained sections. In these preparations, neurons were distinguished from glia and endothelial cells by the presence of dark, coarsely stained Nissl substance in the cytoplasm, a large nucleus, a distinct nucleolus, and lightly stained proximal segments of dendritic processes. In contrast, glial cells lack a conspicuous nucleolus and contain less endoplasmic reticulum.

Interneuron subtypes were identified and counted separately in quantitative analyses. We did not count cell bodies with distinct apical dendrites or pyramidal cytomorphology, such as the CB-ir pyramidal cells that were observed in these anthropoids, as has been previously noted [DeFelipe et al., 1999; Kondo et al., 1999]. Almost all CR-ir interneurons have an ovoid soma shape and correspond to either bipolar or double-bouquet interneurons

[DeFelipe et al., 1999]. PV-ir interneurons, on the other hand, include mostly multipolar chandelier and large basket types [DeFelipe, 1997; Markram et al., 2004]. Populations of CB-ir interneurons, however, are morphologically more heterogeneous [DeFelipe, 1997; DeFelipe et al., 1999]; therefore, we further classified CB-ir cells according to the shape of the soma as either 'ovoid' or 'multipolar'. The ovoid category included small- to medium-sized round interneurons, putatively corresponding to double-bouquet cells. The multipolar category included medium- to large-sized cells with more than two proximal dendrites exiting the cell soma, putatively corresponding to chandelier cells, large basket cells, small basket cells, or other multipolar types.

Stereological Analyses

Our goal was to examine a broad range of species to determine scaling rules for interneurons in the visual cortex. For some cases, however, we were not able to obtain samples that exhaustively covered the full extent of V1 and V2. Therefore, it was not feasible to apply strict stereological sampling to estimate total neuron numbers in each cortical area. Instead, we used the optical disector method to calculate cell densities and to collect a sample population of neurons for cellular volume measurements. Quantification of cellular densities and volumes within layer II/III were performed using a computerized stereology system consisting of a Zeiss Axioplan 2 photomicroscope equipped with a Ludl XY motorized stage, Heidenhain z-axis encoder, an Optronics MicroFire color videocamera, a Dell PC workstation, and StereoInvestigator software (MicroBrightField, Wiliston, Vt., USA). Beginning at a random starting point, three sections equidistantly spaced between 1,200 and 2,000 μm were selected for analysis for each neuronal marker in each cortical region. Densities of neurons were evaluated using the optical disector combined with a fractionator sampling scheme [West et al., 1991; Mouton, 2002]. Optical disector frames (30 \times 30 μm for Nissl stain; 65 \times 65 μm for calcium-binding proteins) were placed in a systematic random fashion to cover the region of interest with approximately 30 frames per section with the exact spacing of disectors depending on the size of the brain. Disector analysis was performed under Koehler illumination using a 63 \times objective (Zeiss Plan-Apochromat, N.A. 1.4). Each cell type was counted when its centroid was located within the optical disector frame according to standard stereologic principles [Howard and Reed, 1998; Mouton, 2002]. The thickness of optical disectors was consistently set to 6 μm to allow for a minimum 2 μm guard zone on either side of the section after z-axis collapse from histological processing. On average, the coefficient of error [Schmitz and Hof, 2000] of optical disector analyses was 0.05 for total Nissl-stained neurons, 0.10 for CB-ir interneurons, 0.09 for CR-ir interneurons, and 0.11 for PV-ir interneurons.

Cellular density (N_V) was calculated as the sum of neurons counted with the optical disectors (ΣQ^-), divided by the product of the sum of the disectors examined and the volume of the disector [Howard and Reed, 1998]. Tissue shrinkage in the z dimension was corrected for density measurements by multiplying the height of the disector by the ratio of the sectioned thickness to the number-weighted mean section thickness after mounting and dehydration [Peterson et al., 1999]. The mounted section thickness was optically measured at every 8th disector sampling location. Because shrinkage in the surface area of mounted sections tends

to be minimal [Dorph-Petersen et al., 2001], no corrections were made for the x and y dimensions.

The cellular volumes of CR- and PV-ir interneurons were calculated in 12 individuals representing the phylogenetic diversity of our sample, including New World monkeys (n = 4), Old World monkeys (n = 4), and hominoids (n = 4). Cellular volumes were estimated using the nucleator probe with a vertical design [Gundersen, 1988]. Neurons were selected for volume measurement in a systematic random fashion by applying optical disector sampling in two sections, as described above. The centroids of neurons included in optical disectors were marked and two transect lines from randomly selected directions were centered at the marker and superimposed over the neuron. The intersection of each line with the outer surface of the neuronal soma was marked and cellular volume was measured based on the nucleator principle [Gundersen, 1988]. This sampling scheme resulted in the measurement of cellular volumes in an average of 55 (range = 32–90) neurons of each immunoreactive type for each cortical area per individual.

Statistical Analyses

Because of the possible confound of differential tissue shrinkage across the sample, our statistical tests focused on questions that circumvent this potential problem. One set of statistical analyses was performed using the percentage of the total layer II/III Nissl-stained neuron population represented by each interneuron subtype. In such ratios, the error from shrinkage is equal in the numerator and denominator and so is mathematically factored out. Analyses of scaling relationships employed reduced major axis (RMA) to determine the slope of the best-fit line to bivariate plots of interneuron subtype densities against total neuron density. In these bivariate plots, both dependent and independent variables contain similar error from fixation artifact. As a result, individual data points might shift along the major axis of the regression, but slope calculations are not altered. RMA techniques provide a superior estimate of the line of best fit to the relationship between two variables (i.e., the main axis along which two variables are correlated) compared to ordinary linear regression because in RMA the residual variance is minimized in both x and y dimensions, rather than the y dimension only [Sokal and Rohlf, 1995]. Genus means were used for all scaling analyses. Data were logarithmically (base 10) transformed prior to RMA line-fitting to fulfill assumptions of normality and homoscedasticity and to facilitate allometric interpretation of slopes. All RMA routines and tests were calculated using (S)MATR software version 1.0 (Falster DS, Warton DI, and Wright IJ; <http://www.bio.mq.edu.au/ecology/SMATR>). Comparisons of RMA slopes and intercepts among groups were performed following the methods described in Warton and Weber [2002].

As a further step in our allometric analyses, we also examined the effect of phylogenetic relatedness on scaling relationships. The method of independent contrasts (IC) accounts for non-independence of data due to shared common ancestry by computing pairwise scores that represent character evolution that has occurred since the common ancestor of sister lineages [Felsenstein, 1985; Garland et al., 1992]. Independent contrasts were calculated using the PDAP:PD TREE module of Mesquite software version 1.06 [Garland et al., 1999; Garland and Ives, 2000]. Standardized independent contrasts were calculated from log-trans-

formed data based on the Goodman et al. [2005] phylogeny of the primates with *Erythrocebus patas* placed in the tree based on Tosi et al. [2004] (fig. 1) and using a Brownian motion model of character evolution. Branch lengths were transformed according to Pagel's method [1992], which assigns all branch lengths to 1 with the constraint that tips are contemporaneous. We examined the sensitivity of independent contrasts to the choice of branch length transformation by also setting all branch lengths to 1. This alternative method did not significantly alter the results. After standardization, ICs were uncorrelated with their standard deviations, indicating that branch lengths meet the required statistical assumptions [Garland et al., 1992].

We followed scaling analyses with tests to compare the percentages of each interneuron subtype among major phylogenetic groups (i.e., New World monkeys, Old World monkeys, and hominoids). Prior to these analyses, data within each group were tested for normality with the Shapiro-Wilk's *W* test and equality of variance was confirmed with the Brown-Forsythe test. Differences among phylogenetic groups and between cortical areas were examined using a 2-way analysis of variance (ANOVA) with repeated-measures design. In this model, phylogenetic group was considered a between-subjects factor and cortical area was considered a within-subjects factor. Post-hoc tests used Bonferroni corrections for multiple comparisons.

Statistical analyses were performed using Statistica software version 6.0 (StatSoft, Inc., Tulsa, Okla., USA). Statistical significance level was set at $\alpha = 0.05$ (two-tailed).

Results

General Staining Patterns

To determine whether there was a significant effect of fixation method on the immunohistochemical staining results, we used independent-samples *t* tests to analyze differences in the percentage of interneurons immunostained for each calcium-binding protein. We did not find significant differences between immersion-fixed and perfusion-fixed specimens, indicating that interindividual variation in the distribution of interneuron subtypes was not influenced by differences in the fixation method.

Immunostaining against CB, CR, and PV labeled the soma, dendrites, and axons of cells, allowing for recognition of different morphological classes (fig. 2). Immunostained interneurons appeared largely consistent in their morphology and general distributions across the anthropoid species examined. The subpopulation of CB-ir neurons varied in shape, including round, bipolar, and multipolar somata. Most CR-ir interneurons were bitufted or bipolar. PV-ir cells were mainly large multipolar types.

The laminar staining profiles of each calcium-binding protein-ir interneuron subtype differed between vi-

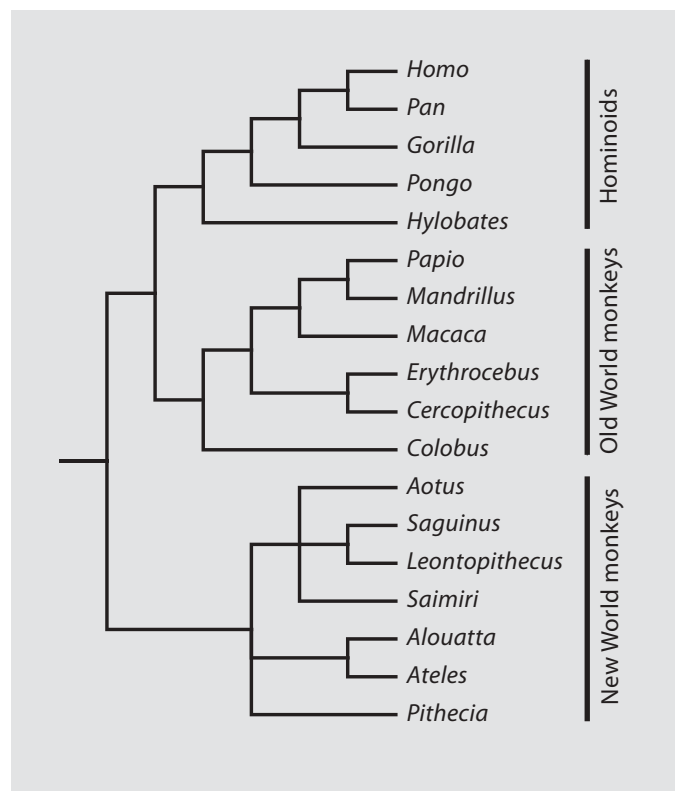


Fig. 1. Phylogenetic tree of the anthropoid primates included in this study.

sual areas (fig. 3). In V1, CB-ir cells were distributed rather diffusely through layers II–VI, with more prominent staining in layers II/III, IVB, IVC and V. Species differences in laminar arrangements of CB immunostaining resembled those described by Preuss and Coleman [2002]. CR-ir neurons in V1 were observed mostly in layers II/III, IVB, and V. A narrow stripe of stained neurons and neuropil was present at the bottom of layer IVB and CR-ir cells were sparser in layer V compared to CB-ir neurons. In area V2, CB- and CR-ir cells were more concentrated in layers II/III than in other layers. The PV-ir neuron subpopulation in V1 was most abundant in layers II/III, IVA, IVC, and VI, with a pronounced band of staining in layer IVC. In area V2, PV-ir cells were dispersed more regularly through layers II–VI. The general appearance of cyto- and chemoarchitecture in V1 and V2 from representative species is shown in figure 4.

Clear staining of CB- and CR-ir double-bouquet axon bundles was observed in all specimens, with more abundant immunoreactive fibers in V2 relative to V1 (fig. 5).

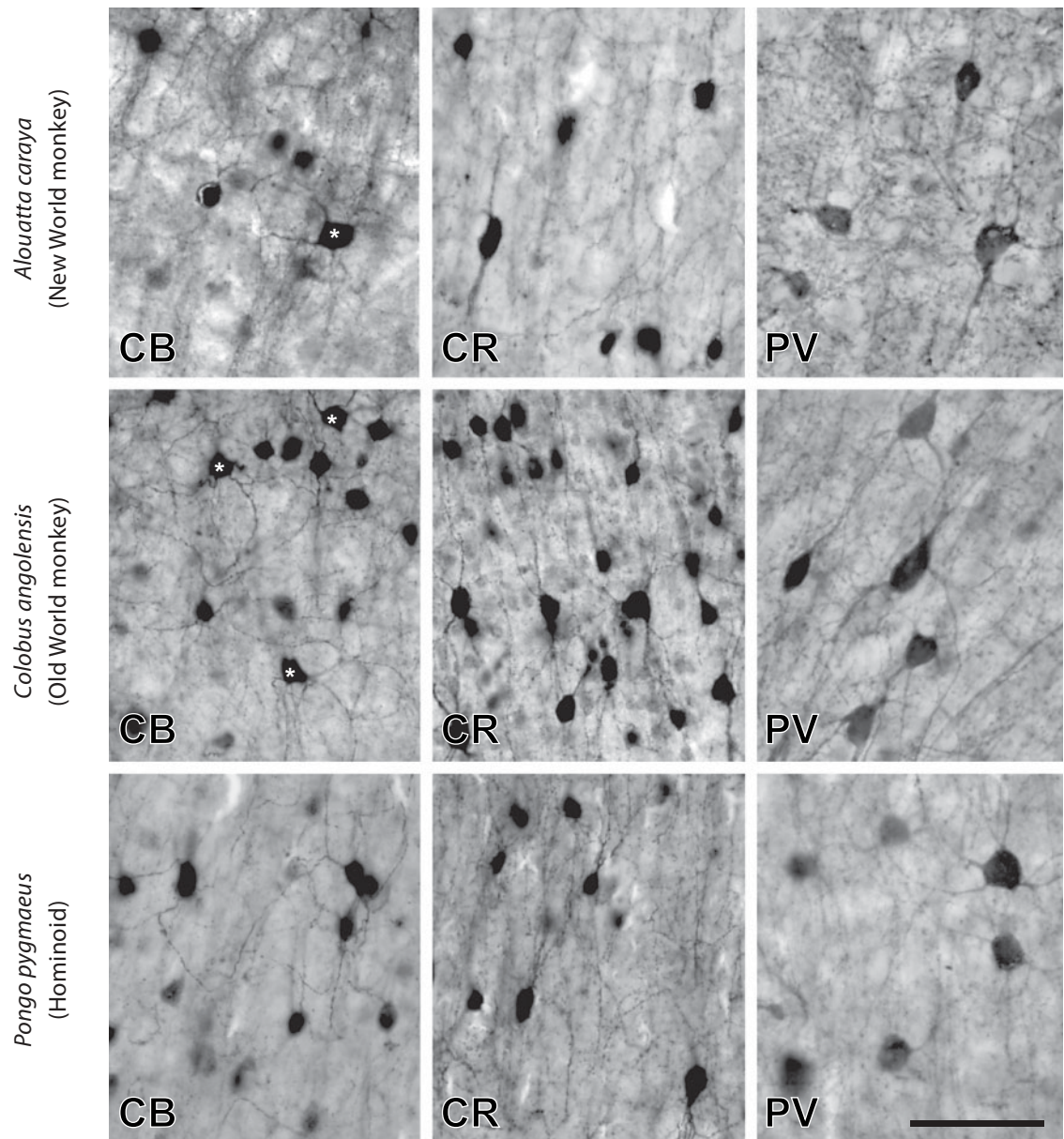


Fig. 2. Examples of calcium-binding protein-containing nonpyramidal interneuron subtypes in layer II/III of area V1 from representative members of major anthropoid groups. Similar cellular morphologies were observed for each calcium-binding protein in all species examined. Calbindin was expressed in neurons with round or ovoid somata and bipolar or bitufted process, as well as some multipolar types (examples indicated by asterisks). Calretinin immunoreactivity was generally observed in somata with round or bipolar shapes. Parvalbumin was found mostly in large multipolar neuron types. Scale bar = 100 μ m.

Overall, across species there was a greater density of CB-ir double-bouquet axons than CR-ir double-bouquet axons. In our hands, cartridges of PV-ir chandelier terminals in layer II/III were only observed in some of the perfusion-fixed materials. When present, they occurred in

greater density in V2 than in V1. Many PV-ir puncta in the neuropil were seen surrounding unstained somata in both visual areas, suggesting that other PV-ir terminals, such as those of basket cells, are abundant.

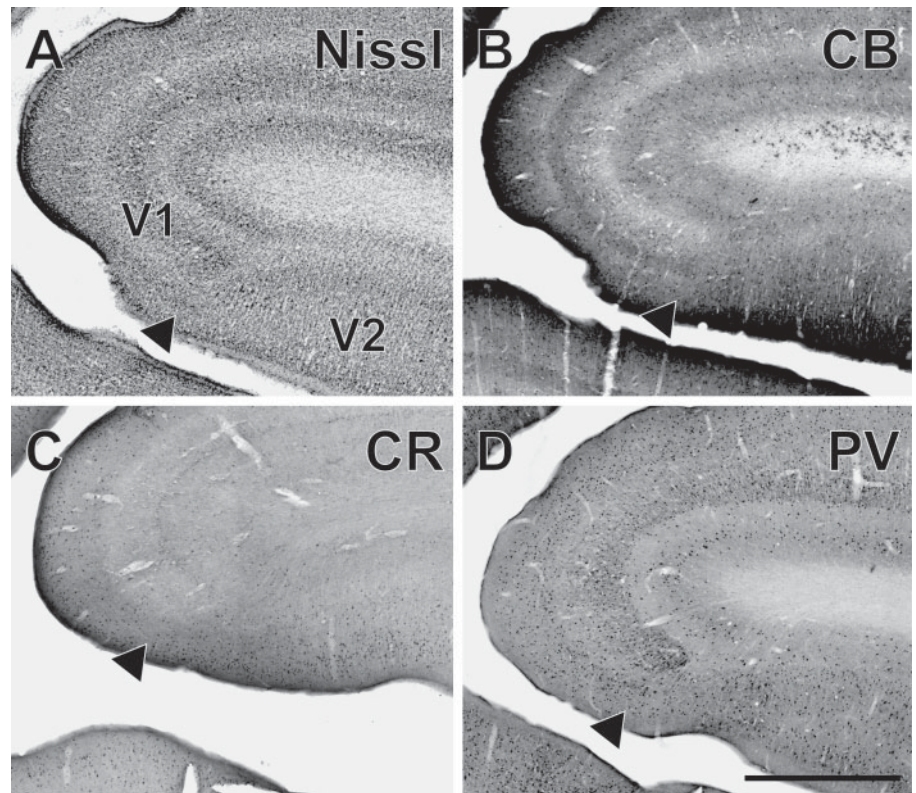


Fig. 3. Adjacent sections from a patas monkey (*Erythrocebus patas*) brain processed for **A** Nissl substance, **B** calbindin, **C** calretinin, and **D** parvalbumin, showing the border between areas V1 and V2 (indicated by arrowheads). Note that high densities of immunoreactivity for calbindin in neurons and neuropil of layer IVB in area V1 abruptly terminates at the border with V2. Likewise, intense parvalbumin immunoreactivity in layer IVC of area V1 also ends at the transition to V2. Scale bar = 1 mm.

Scaling of Total Neuron Density on Brain Weight

The results of stereologic counts of cell densities are shown in table 2. Table 3 shows the scaling slopes of the regressions of total neuron densities against brain weight. Using species data, a common RMA slope described the scaling of total layer II/III neuron density on brain weight for both V1 and V2 (test statistic = 0.03, $p = 0.87$; slope = -0.30 ; lower CI = -0.26 ; upper CI = -0.39). This slope reflects a negative allometric scaling relationship between neuron densities in the visual cortex and brain weight (fig. 6A). That is, as brain size increases, neuron densities in visual cortex decrease at a rate that is slower than changes in brain weight. The elevation of the two regression lines differed such that V2 neuron densities were lower than V1 neuron densities at any given brain weight ($F_{1,33} = 5.20$; $p = 0.03$).

Next we compared slopes from phylogenetic independent contrast (IC) regressions to slopes from species data (table 3). In V2, the IC slope fell below the confidence intervals of the species slope. Most importantly, however, for both V1 and V2 the correlations between brain weight and total neuron densities were not significant when phylogenetic bias was taken into account by using ICs. These

results suggest that the observed correlation between species mean neuron density and brain weight derives from the tendency for close relatives to resemble one another in both traits because they are inherited from a common ancestor, not because of consistent covariance between neuron density and brain weight throughout nodes in the phylogenetic tree.

Scaling of Interneuron Subtype Densities on Total Neuron Density

We plotted the density of each interneuron subtype against total neuron density in layer II/III to assess scaling relationships. We considered local neuron density to be a more appropriate reference variable than brain weight for these analyses because it allows for interpretation of scaling exponents in terms of proportional changes among interneurons within the context of the local processing unit. In this regard, the null hypothesis we were testing was whether interneuron densities scale isometrically (i.e., a slope of 1) with respect to total neuron density. This hypothesis denotes maintenance of a constant ratio of interneuron subtypes across changes in total neuron density. A significant departure from isomet-

Gorilla gorilla(Hominoid)

I
II/III
IV̄A
IV̄B
IV̄C
V̄
VĪ

I
II/III
IV̄
V̄
VĪ

Mandrillus sphinx(Old World monkey)

I
II/III
IV̄A
IV̄B
IV̄C
V̄
VĪ

I
II/III
IV̄
V̄
VĪ

Aotus trivirgatus(New World monkey)

I
II/III
IV̄A
IV̄B
IV̄C
V̄
VĪ

I
II/III
IV̄
V̄
VĪ

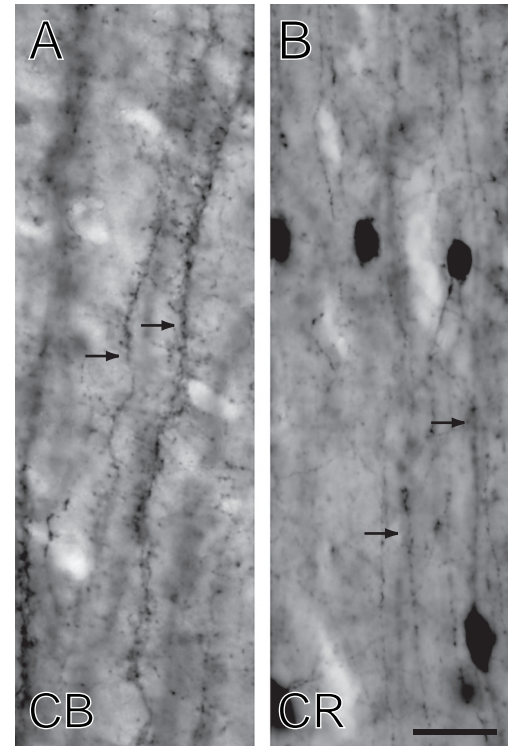


Fig. 5.Examples of A calbindin- and B calretinin-immunoreactive double-bouquet axon bundles (indicated by arrows) from area V2 of a black howler monkey(*Alouatta caraya*). Among all species, calbindin-immunoreactive double-bouquet axon bundles were denser than those stained for calretinin, and double-bouquet axon bundles were more frequent in V2 than V1. Scale bar = 25 μ m.

Fig. 4.Cyto- and chemoarchitectural staining patterns in V1 and V2 of representative members of major anthropoid groups. Scale bar = 50 μ m.

Table 2. Results of stereologic estimates of cellular densities in layer II/III (genus mean cells per mm³)

Species	N	Brain weight, g	Area V1					CR	PV
			total neurons	CB	CB ovoid	CB multipolar	CB		
<i>Homo sapiens</i>	2	1,219.0	160,320	4,971	4,129	842	11,680	8,917	
<i>Pan troglodytes</i>	2	303.2	210,938	7,801	7,172	630	7,669	7,386	
<i>Gorilla gorilla</i>	2	515.7	136,984	7,193	5,673	1,520	8,435	5,898	
<i>Pongo pygmaeus</i>	2	342.7	177,535	4,839	4,123	716	9,869	5,349	
<i>Hylobates muelleri</i>	1	101.8	200,892	7,999	7,163	836	6,250	16,304	
<i>Papio anubis</i>	2	155.8	357,279	14,425	11,428	2,997	19,209	18,108	
<i>Mandrillus sphinx</i>	1	159.2	269,180	14,904	11,656	3,248	30,406	15,488	
<i>Macaca maura</i>	2	90.6	377,210	26,391	21,473	4,918	22,763	12,043	
<i>Erythrocebus patas</i>	2	102.3	423,202	24,039	21,560	2,480	29,157	15,652	
<i>Cercopithecus kandti</i>	1	71.6	249,733	18,495	16,629	1,867	13,545	19,313	
<i>Colobus angolensis</i>	1	74.4	252,894	19,442	13,161	6,281	18,894	14,026	
<i>Alouatta caraya</i>	1	55.8	197,649	13,845	12,631	1,214	21,517	11,700	
<i>Ateles geoffroyi</i>	1	103.0	207,008	7,908	7,583	325	11,813	6,012	
<i>Saimiri</i> sp.	2	22.7	469,672	41,500	31,344	10,156	35,037	21,334	
<i>Aotus trivirgatus</i>	1	13.2	547,483	30,551	16,451	14,101	31,133	10,689	
<i>Saguinus oedipus</i>	1	10.0	319,444	30,675	21,498	9,176	32,479	13,650	
<i>Leontopithecus rosalia</i>	2	12.2	252,902	9,246	7,698	1,548	17,743	11,951	
<i>Pithecia pithecia</i>	1	30.0	196,451	18,682	11,642	7,040	18,885	14,511	

Table 3. Slope estimates and correlation coefficients for scaling relationships from genus means (n = 18)

Independent variable	Dependent variable	Species data					Independent contrasts		
		r	RMA slope	lower 95% CI	upper 95% CI	p	r	RMA slope	p
Brain weight	V1 total neuron density	-0.586	-0.29	-0.44	-0.19	0.01*	-0.355	-0.44	0.15
	V2 total neuron density	-0.562	-0.31	-0.46	-0.20	0.01*	-0.225	-0.50	0.37
V1 total neuron density	V1 CB density	0.815	1.68	1.24	2.27	0.00*	0.619	1.73	0.01*
	V1 CB ovoid density	0.788	3.47	2.15	5.58	0.00*	0.586	1.68	0.01*
	V1 CB multipolar density	0.358	1.55	1.12	2.13	0.14	0.094	4.26	0.71
	V1 CR density	0.757	1.38	0.98	1.94	0.00*	0.466	1.38	0.05*
	V1 PV density	0.561	1.12	0.73	1.71	0.02*	0.128	1.11	0.61
V2 total neuron density	V2 CB density	0.745	1.74	1.23	2.47	0.00*	0.421	1.31	0.08
	V2 CB ovoid density	0.716	2.97	1.97	4.49	0.01*	0.341	1.42	0.17
	V2 CB multipolar density	0.600	1.74	1.21	2.50	0.00*	0.312	3.29	0.21
	V2 CR density	0.824	1.10	0.81	1.47	0.00*	0.717	1.07	0.00*
	V2 PV density	0.768	1.07	0.76	1.49	0.00*	0.584	0.91	0.01*

Boldface type indicates cases where the species mean slopes for interneuron scaling does not include isometry (i.e., slope of 1) within the 95% confidence intervals. * = Statistically significant.

ric scaling would suggest that the particular interneuron subtype changes in its proportionate representation as neuron density varies across species. The scaling exponents for regressions of the density of each interneuron

subtype on total neuron density are shown in table 3. Using species values, the slopes for most interneuron subtypes included isometry within their confidence intervals, although all estimated slope were greater than 1. In

Area V2					
total neurons	CB	CB ovoid	CB multipolar	CR	PV
114,695	3,796	3,113	684	10,603	7,828
123,713	4,871	4,670	201	8,600	6,327
113,467	5,176	3,767	1,410	12,436	4,376
149,676	4,741	3,777	963	8,890	4,548
173,504	4,808	4,508	301	9,930	7,880
310,483	17,353	12,275	5,078	23,764	18,110
161,265	16,150	13,554	2,595	22,116	9,890
298,556	18,564	13,359	5,205	19,539	14,421
345,080	25,568	22,877	2,691	32,780	15,392
174,457	30,506	27,733	2,773	12,983	14,548
181,633	15,841	11,074	4,768	22,024	9,169
187,678	8,556	5,254	3,302	16,945	9,798
187,963	11,832	11,547	285	12,052	5,771
350,716	38,199	29,222	8,977	28,509	18,684
468,562	24,441	17,063	7,378	34,216	12,856
219,733	16,993	11,167	5,826	25,400	10,780
184,296	7,688	6,454	1,234	16,606	9,826
149,184	13,116	8,284	4,832	12,974	8,498

contrast, significant positive allometry characterized the scaling of all CB-ir interneuron subtypes in V1 and V2 (fig. 6).

When scaling relationships were calculated with ICs, however, several relationships became non-significant (table 3). Of those remaining, most of the IC slopes fell within the 95% confidence intervals of the slopes calculated with species data. The only exception was V1 CB-ir ovoid interneurons, which had a lower IC slope compared with the species slope estimate.

Because differences in the strength of correlation between species data and IC data suggest that the majority of covariance is at the level of higher-order taxonomic groups, we tested for differences among New World monkeys, Old World monkeys, and hominoids in slopes and intercepts for species data. If present, evidence of differences among phylogenetic groups in the y-axis elevation of the line, but not the slope, indicates a 'grade shift' wherein the proportional relationship between variables has been modified in the evolution of taxa, while the scaling between variables is preserved [Harvey and Krebs, 1990; Purvis and Webster, 1999]. We found no significant scaling differences among phylogenetic groups for any interneuron subtype in either area, except for total CB-ir interneuron density in V2 ($F_{2,14} = 6.39$; $p = 0.01$). Post-hoc Tukey-Kramer tests revealed a significantly lower elevation of the RMA line in hominoids

compared to Old World monkeys ($p < 0.01$). These results should be considered tentative, however, because our data contain relatively small numbers of species within each phylogenetic group, thereby increasing the likelihood of type I error in statistical detection of scaling differences.

Next we tested whether species slopes for each interneuron subtype differed between V1 and V2 across the entire anthropoid sample. None of the likelihood ratio tests were significant, indicating that interspecific changes in the density of each interneuron subtype are governed by a common scaling pattern in both V1 and V2.

Percentages of Neuron Subtypes among Phylogenetic Groups

To examine the consequences of these scaling patterns, we analyzed variation in the percentage of each interneuron subtype among phylogenetic groups using data from all individuals in a 2-way repeated measures ANOVA design (fig. 7). The percentages of each interneuron subtype in layer II/III of V1 and V2 are shown in table 4. We calculated separate models for each interneuron subtype using phylogenetic group as the between-subjects factor and cortical area as the within-subjects factor. The only models showing significant phylogenetic group differences were CB-ir interneuron subtype per-

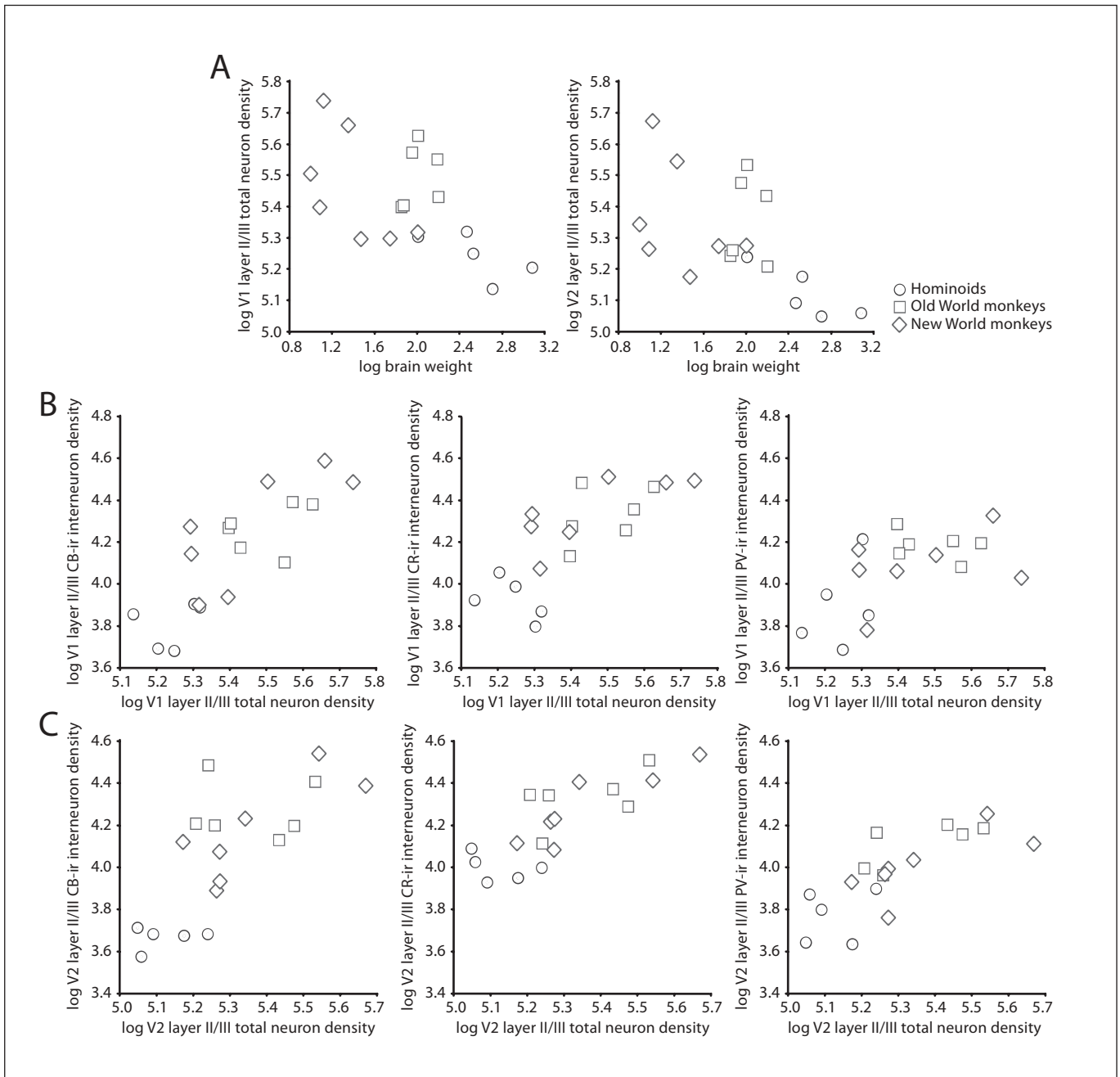


Fig. 6. Plots showing the scaling of **A** genus mean layer II/III visual cortex neuron density on brain weight, **B** genus mean layer II/III V1 interneuron subtype densities on total V1 neuron density, and **C** genus mean layer II/III V2 interneuron subtype densities on total V2 neuron density.

centages. There were no significant interaction effects. The percentage of total CB-ir interneurons ($F_{2,24} = 5.59$; $p = 0.01$), CB-ir ovoid interneurons ($F_{2,24} = 4.43$; $p = 0.02$), and CB-ir multipolar interneurons ($F_{2,24} = 3.36$; $p = 0.05$) all displayed a significant effect of phylogenetic

group. The significant contrasts revealed by post-hoc Bonferroni corrections for multiple comparisons are shown in figure 7.

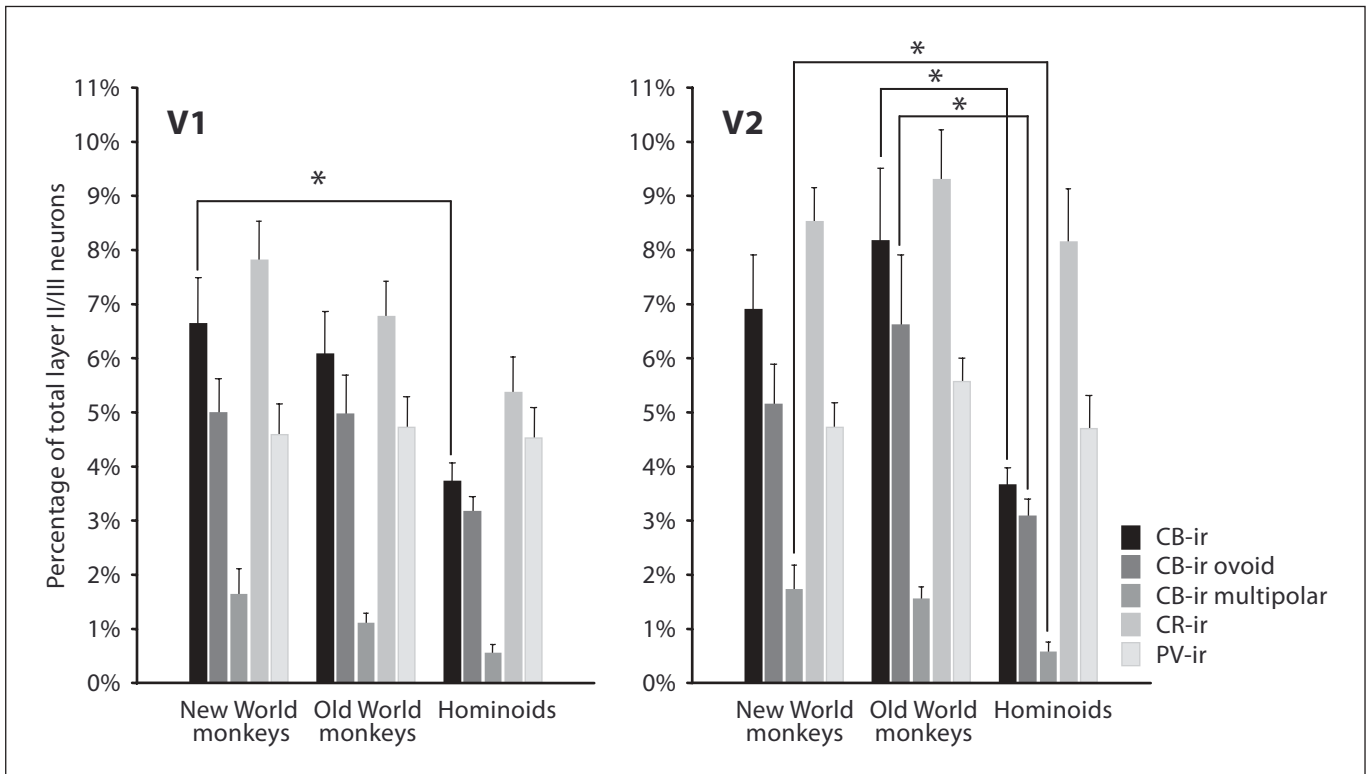


Fig. 7. Bar graphs showing differences among phylogenetic groups in the percentage (mean \pm SE) of somata immunostained for different interneuron subtypes in layer II/III of V1 and V2, relative to the total Nissl-stained neuron population. All pairwise contrasts that are significant after post-hoc Bonferroni correction are shown with asterisks.

Table 4. The percentage of the total layer II/III neuron population represented by each interneuron subtype

Area	Interneuron subtype	New World monkeys (n = 9)		Old World monkeys (n = 9)		Hominoids (n = 9)	
		mean	SEM	mean	SEM	mean	SEM
V1	CB	6.6	0.9	6.1	0.8	3.7	0.3
	CB ovoid	5.0	0.7	5.0	0.7	3.2	0.3
	CB multipolar	1.6	0.5	1.1	0.2	0.6	0.2
	CR	7.8	0.7	6.8	0.7	5.4	0.7
	PV	4.6	0.6	4.7	0.6	4.5	0.6
	CaBP total	19.1	1.7	17.6	1.5	13.6	1.0
V2	CB	6.9	1.1	8.2	1.4	3.7	0.3
	CB ovoid	5.2	0.8	6.6	1.3	3.1	0.3
	CB multipolar	1.7	0.5	1.6	0.2	0.6	0.2
	CR	8.5	0.7	9.3	1.0	8.1	1.0
	PV	4.7	0.5	5.6	0.4	4.7	0.6
	CaBP total	20.2	1.8	23.1	2.0	16.5	1.6

CaBP = Calcium-binding protein.

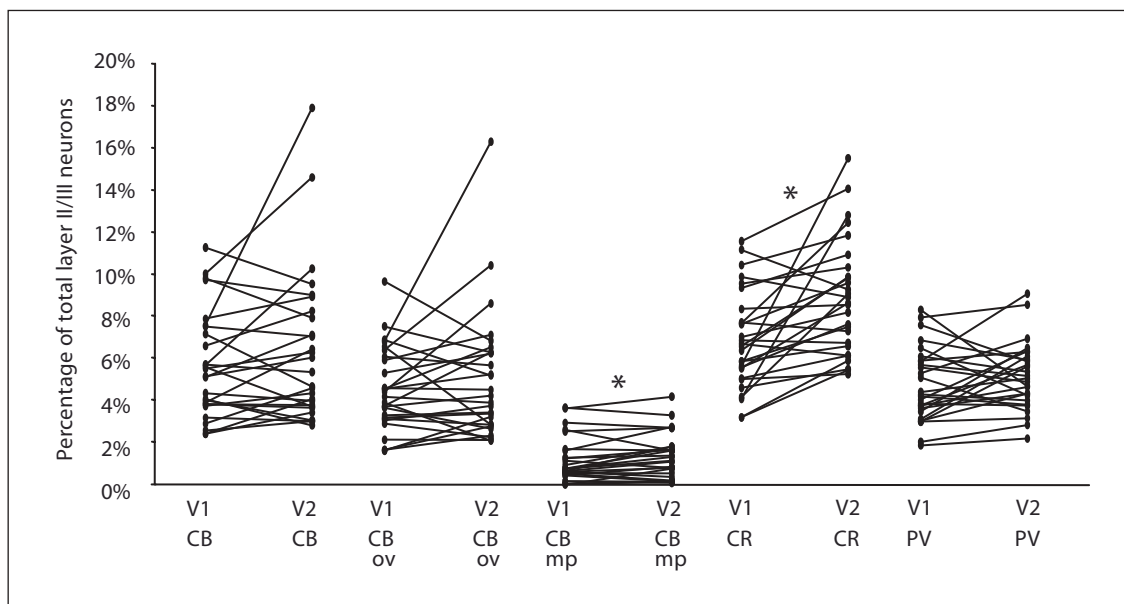


Fig. 8. Graph showing the within-individual change in the percentage of each layer II/III interneuron subtype between V1 and V2. Asterisks indicate interneuron subtypes that show a significant within-subjects effect in the ANOVA model. ov = Ovoid; mp = multipolar.

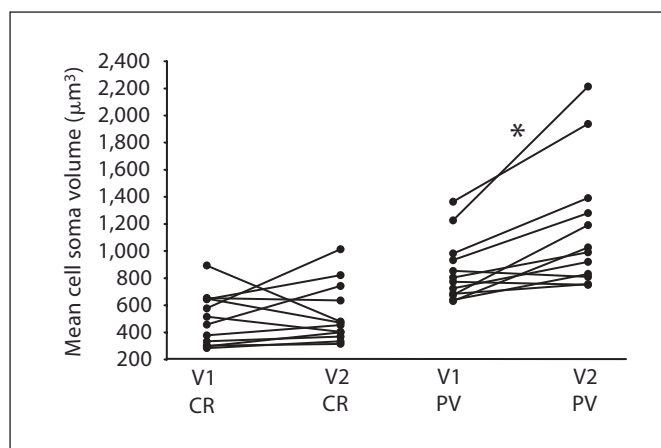


Fig. 9. Graph showing the within-individual change in the mean soma volumes of layer II/III calretinin- and parvalbumin-immunoreactive interneurons between V1 and V2. Asterisks indicate significant contrasts from dependent-samples t tests.

Differences in Proportions and Volumes of Interneuron Subtypes between V1 and V2

The within-subjects term in the two-way repeated measures ANOVA model indicates differences in interneuron percentages between V1 and V2 within individuals. The percentage of CB-ir multipolar interneurons ($F_{2,24} = 4.43$; $p = 0.05$) and CR-ir interneurons ($F_{2,24} = 17.21$; $p < 0.01$) differed significantly between visual areas. Within individuals, V2 tended to contain greater

proportions of these interneuron subtypes relative to V1 (fig. 8).

To examine whether consistent changes of mean cell volumes of CR- and PV-ir characterize the transition from V1 to V2 within individuals, we used dependent-samples t tests (table 5). The mean cell volume of PV-ir interneurons was significantly greater in V2 than in V1 ($t_{11} = -3.80$; $p < 0.01$), whereas CR-ir cell volumes did not differ between areas ($t_{11} = -0.61$; $p = 0.56$) (fig. 9).

Table 5. Mean cell soma volumes (μm^3)

Species	CR		PV	
	V1	V2	V1	V2
<i>Homo sapiens</i>	573	1,007	1,225	2,211
<i>Gorilla gorilla</i>	640	818	848	804
<i>Pongo pygmaeus</i>	643	469	800	986
<i>Hylobates muelleri</i>	453	736	679	753
<i>Mandrillus sphinx</i>	294	395	669	1,187
<i>Macaca maura</i>	280	331	638	826
<i>Erythrocebus patas</i>	299	313	719	917
<i>Colobus angolensis</i>	511	402	977	1,386
<i>Alouatta caraya</i>	888	476	1,359	1,935
<i>Saimiri boliviensis</i>	375	449	771	745
<i>Aotus trivirgatus</i>	647	632	626	1,024
<i>Leontopithecus rosalia</i>	331	363	927	1,278

Discussion

We have examined calcium-binding protein-containing interneurons in the visual cortex of diverse anthropoid primate species. Our results demonstrate that V1 and V2 exhibit phylogenetic variation in the relative distribution of inhibitory interneuron subtypes in layer II/III, with a reduced proportion of CB-ir interneurons in hominoids as compared to New World monkeys and Old World monkeys. Comparisons of interneurons in layer II/III between visual areas, furthermore, revealed a trend across species for V2 to have greater proportions of CB-ir multipolar interneurons and CR-ir interneurons, as well as larger mean soma volumes of PV-ir cells, relative to V1.

Methodological Considerations

In this study we classified interneuron subtypes according to single-label immunohistochemical staining for CB, CR, and PV. It is worth noting, however, that some cortical interneurons co-express more than one calcium-binding protein. For example, colocalization between CB and CR, CB and PV, and CR and PV in interneurons of adult primates and rodents has been observed [Van Brederode et al., 1990; Kubota and Jones, 1993; del Rio and DeFelipe, 1996, 1997a, b; Gonchar and Burkhalter, 1997; Leuba and Saini, 1997; Morrison et al., 1998]. In all taxa examined, however, the number of neuronal somata that contain multiple calcium-binding proteins represents a very small subpopulation of the cells that express any single calcium-binding protein. The greatest degree of calcium-binding protein colocalization has been reported for PV-ir cells in layers V and VI of the human temporal

cortex, where approximately 14% also contain CB [del Rio and DeFelipe, 1997a]. However, studies in V1 and V2 of humans and macaques have found calcium-binding protein colocalization in less than 7.5% of neurons immunoreactive for any single marker [Van Brederode et al., 1990; Leuba and Saini, 1997]. Thus, although our calculations of interneuron densities certainly contain a degree of error because of overcounting the subpopulation of calcium-binding protein-colocalizing neurons, this error is most likely quite minimal.

Our determination of different morphological classes of CB-ir interneurons might also contain a degree of error due to the subjective nature of their categorization. Nevertheless, scaling exponents for CB-ir neurons always exceeded isometry, whether counted as a total population or divided into ovoid and multipolar subclasses.

The Influence of Phylogeny on Scaling

For many of the bivariate scaling relationships we analyzed, both species data and IC data yielded significant and similar scaling exponents (table 2). This congruence indicates that contemporary species values provide a reliable gauge of allometric rules that apply regardless of evolutionary history and affinities. Indeed, a correspondence between species and IC slopes tends to occur when traits scale in a constant manner across the entire phylogenetic tree, even in the presence of outlier points that represent y-axis grade shifts [Nunn and Barton, 2001]. Nevertheless, we found little evidence of grade shifts from our species data analyses. Therefore, scaling relationships that did not display phylogenetic bias might be interpreted as being more strongly determined by scaling rules rather than by phylogenetic effects such as adaptation or inertia. In this regard, our data indicate that the density of V1 CB-ir ovoid interneurons, V1 and V2 CR-ir interneurons and V2 PV-ir interneurons regularly vary with respect to total neuron density.

The apparent correlations between other neuroanatomical variables based on species values, however, were not significant after ICs were calculated as a control for phylogeny. This was the case for: V1 and V2 total neuron density versus brain weight, V1 multipolar CB-ir interneuron density and PV-ir interneuron density versus total neuron density as well as all V2 CB-ir interneuron subtype densities versus total neuron density. In general terms, this discrepancy in species and IC correlations indicates that the two traits in question do not display consistent covariance at multiple nodes in the phylogenetic tree. This might take place when a large portion of covariance in the crown species data is due to strong trait

correlation that occurred at few branching events early in the phylogeny, a pattern characteristic of adaptive radiations [Price, 1997]. In this mode of evolutionary diversification, highly correlated changes among traits take place in the basal members of higher-order taxonomic groups, and then subsequent species diversification occurs with much weaker correlated trait evolution. Although analysis of species data can achieve statistically significant line-fitting, an actual scaling relationship does not exist, but rather a spurious correlation that is caused by the confounding of phylogenetic relatedness and size. Most importantly, this implies that there is little functional or architectural constraint to impel traits to evolve in a correlated fashion repeatedly throughout the phylogenetic tree. In our data, the clearest example of this type of confound can be seen in the plots of total neuron density against brain weight for both visual areas (fig. 6A). When such incongruence between species and IC correlations exists, phylogenetic affinities and evolutionary adaptations are likely to represent more important determinants of apparent scaling in species data than any functional allometric constraints. It should be noted, however, that disparities between species and IC correlations could also arise from methodological sources such as unrepresentative species means due to small sample size or error in the phylogenetic tree topology [Purvis and Webster, 1999].

General Scaling Patterns

Although evaluating phylogenetic bias is necessary to illuminate the underlying causes of observed interspecific scaling relationships, insight into the functional implications of size-related changes across species might be obtained by examining allometric exponents. Ultimately, a host of physical, electrochemical, and molecular design constraints collectively determines allometric changes in the brain, some of which occur to maintain functional equivalence and some of which might entail important computational modifications.

Based on species data, we found that total layer II/III neuron densities in V1 and V2 scale against brain weight with a common negative allometric slope of -0.30 , displaying lower densities in V2 compared to V1. On average, neurons in V1 are 1.31 times denser than in V2. In other studies of species data from diverse mammals, it has been demonstrated that neuron density in various cortical areas also decreases relative to brain size with a scaling exponent of approximately -0.3 [Tower, 1954; Prothero, 1997]. These empirical findings fit with a model predicting that a constant average percent intercon-

nectedness among neurons cannot feasibly be sustained with increasing gray matter volume, so the reach of processing networks does not keep pace with brain size variation [Changizi, 2001]. It is significant that we found that neuron density scales against brain weight with this same allometric exponent in the current study, especially given the possibility that phylogenetic effects might influence this relationship as discussed above. This implies that architectural rules generally govern neuron density scaling with brain size change across the cortex of mammals; but there is enough latitude in these rules such that neuron density might be relatively unlinked to brain size when comparisons are made among close relatives. Indeed, studies of prefrontal cortex (area 13) and primary motor cortex (area 4) of hominoids also show that neuron densities vary independently of overall brain size within this restricted phylogenetic range [Sherwood and Hof, in press]. Interspecific variation in the factors underlying neuron density, such as cell soma size, the degree of dendritic arborization, and glial size and density, therefore, could reflect evolutionary adaptations within lineages in a regionally specific manner.

With regard to differences between visual areas, we found that neuron density scaling against brain weight in V2 has a lower y-axis elevation than in V1. Consistent with our results, studies of visual cortex pyramidal neurons in primates have shown that the extent of the basal dendritic tree and density of spines is greater in V2 than V1, and increases in these parameters are associated with larger brain size at equal allometric rates in both areas [Elston et al., 2006]. Taken together with the current results, these data suggest that a constant difference of overall network interconnectedness is maintained between V1 and V2 in anthropoid primates across a large diversity in brain size.

Scaling Patterns of Interneurons and Phylogenetic Variation

We calculated the scaling of various interneuron subtype densities against total neuron density in V1 and V2. Because of the unbiased nature of the stereologic sampling design, these cell counts were not influenced by potential variation in interneuron densities among cytochrome oxidase (CO)-rich blobs, stripes, or non-CO-rich modules [Hendry and Carder, 1993]. Although most interneuron subtypes displayed statistically isometric scaling patterns against total neuron density, CB-ir interneuron subtypes were characterized by a positive allometric scaling relationship. Thus, although most other components of the local microcircuitry maintain a constant pro-

portional representation among the total neuron population, CB-ir interneurons become relatively less dense with decreases in total neuron density which characterizes hominoids. Furthermore, because many of the CB-ir interneuron density regressions exhibit phylogenetic bias, with data from New World monkeys and Old World monkeys overlapping in scatterplots (fig. 6B, C), the evidence suggests that early hominoids were evolutionarily derived in having a relative reduction of CB-ir interneurons in layers II/III of visual cortex.

Can the current observations of interneuron scaling be generalized to other neocortical areas, or is this pattern representative only of V1 and V2? Although other studies have not directly addressed the scaling relationships of interneurons, several have reported percentages of interneurons relative to the total neuron population. As a result of the distinctive positive allometric scaling of CB-ir interneuron subtypes, we found that these cells represent a smaller percentage of the total layer II/III neuron population in the visual cortex of hominoids. By contrast, in a previous study we found a greater percentage of PV-ir interneurons in layers III and V in the region of orofacial representation of primary motor cortex in hominoids relative to Old World monkeys, whereas CB- and CR-ir interneurons did not show a significant difference among these taxa [Sherwood et al., 2004]. In another study, Gabbott et al. [1997b] reported that humans and long-tailed macaque monkeys have a similar percentage of CR-ir interneurons in medial prefrontal cortex (area 32). Collectively, these data demonstrate that different components of the inhibitory neuron population might vary across anthropoid primate species depending on the cortical area. These observations run counter to the widespread view that the cellular organization of cortical columns is relatively uniform across areas and species [Rockel et al., 1980].

Functional Implications of Interspecific Variation

The connectivity of the various inhibitory interneuron subtypes is particularly significant in the context of the columnar organization of the neocortex [Douglas and Martin, 1992; Mountcastle, 1997]. CB- and CR-ir double-bouquet and bipolar cells have vertically-oriented axonal arbors [DeFelipe, 1997; Ballesteros-Yanez et al., 2005] that provide dendrite-targeting inhibition at different layers to synchronize the activity of pyramidal neurons across various levels within a narrow cortical domain [DeFelipe et al., 1989]. Accordingly, changes in the proportionate representation of these interneurons might affect physiological responses within and among neigh-

boring minicolumns. If the reduction of layer II/III CB-ir somata in hominoids corresponds to fewer double-bouquet and bipolar interneurons, this suggests that there is less vertical inhibition of pyramidal neuron activity. It is also possible that the relative decline of CB immunoreactivity in hominoids is not due to loss of any GABAergic interneurons, but instead reflects changes in the electrophysiological phenotype of a subset of interneurons such that the cells that co-express CB with CR, vasoactive intestinal peptide, or cholecystokinin [Markram et al., 2004] have lost their bursting discharge behavior. It would be difficult, however, to directly extrapolate regarding the disposition of inhibitory microcircuitry based on neuron soma counts. Recent evidence shows that despite similarities in the general somatic morphology of CB-ir neurons among mammalian species, CB-ir axon bundles can display phylogenetic variability [Ballesteros-Yanez et al., 2005]. Of note, CB immunostaining of double-bouquet axon bundles was observed most prominently in certain neocortical areas of primates and in visual cortex of carnivores although this trait was not present in rodents, lagomorphs, or artiodactyls. In any event, the current findings of variation among primates in visual cortex histological organization are consistent with other studies demonstrating that features of cortical microstructure within homologous cortical areas display phylogenetic diversity [e.g., Glezer et al., 1993; Semendeferi et al., 1998, 2001; Hof et al., 1999; Preuss et al., 1999; Preuss and Coleman, 2002; Sherwood et al., 2003, 2004; Hutsler et al., 2005].

Functional Implications of Variation between Visual Areas

Our comparative quantitative study of interneuron distributions in V1 and V2 also permitted us to address whether there are invariant changes of interneuron proportions and soma volumes that consistently occur between these different hierarchical levels of visual processing. We found a trend within individuals across all species for V2 to contain greater percentages of CB-ir multipolar and CR-ir interneurons, as well as larger mean soma volumes of PV-ir cells in comparison to V1.

Several aspects of physiology, retinotopy, and architecture have been shown to distinguish V1 and V2 in anthropoids [Rosa and Krubitzer, 1999; Lee, 2003; Sinich and Horton, 2005]. Neurons in V2 combine streams of visual information that remain segregated in V1 by allowing interactions among cells with different stimulus selectivities and by integrating stimulus features

across larger regions of the visual field [Boynton and Hegde, 2004]. Along with increasingly larger receptive field sizes through occipitotemporal visual areas [Allman and Kaas, 1971; Felleman and Van Essen, 1991; Van Essen et al., 1992], several architectural changes have also been noted to occur with anterior progression through hierarchical levels of the visual cortex in primates. In macaque monkeys, supragranular CB-ir pyramidal neurons become gradually more numerous in higher-order visual areas [Kondo et al., 1994]. In addition, studies from several different primate species show that pyramidal neurons in V2 have more extensive dendritic arbors with a higher density of spines than those in V1 [Lund et al., 1993; Elston et al., 1996, 2005; Elston and Rosa, 1997; Elston, 2003]. In humans, V1 differs from V2 in the laminar densities of several receptors, including inhibitory GABA_A receptors [Zilles et al., 2004]. In the present study, we found a greater percentage of CB- and CR-ir interneuron subtypes in V2 compared to V1, which matched our qualitative observation of increased density of CB- and CR-ir double-bouquet axon bundles. Hence, it appears that modifications of supragranular vertical intracolumnar inhibition might also be important in defining properties of neuronal activity within these different visual areas.

The selective increase in the somatic volume of PV-ir interneurons, on the other hand, could reflect changes in patterns of lateral inhibition between visual areas. Injections of biocytin in macaque monkeys label terminal zones with a larger patch size and larger center-to-center distance between patches in area V2 relative to V1 [Lund et al., 1993]. It has been shown that the horizontal extent of PV-ir large basket cell axons correspond closely to the size of the inter-patch territory and therefore might be critical to the development of the inhibitory surround encircling each pyramidal neuron [Lund et al., 1993]. Large basket cells have horizontally extended axons that target the perisomatic region of pyramidal cells across different cortical columns [Lund and Lewis, 1993; Somogyi et al., 1998]. In a similar manner, PV-ir chandelier cells also inhibit the firing of pyramidal neurons in different horizontal positions by forming strings of synapses on the axon initial segment on postsynaptic neurons. Thus, the various classes of PV-ir interneurons are important in structuring lateral inhibition to shape and fine-tune receptive fields [Wang et al., 2000a, b; Li et al., 2002]. The inter-regional differences in PV-ir interneuron cell volumes, therefore, might reflect increased length of axonal projections or increased cellular requirements for metabolism and protein synthesis.

Conclusion

In summary, this study demonstrates that the inhibitory interneurons of layer II/III visual cortex in anthropoid primates exhibit taxonomic differences, specifically in displaying relatively lower proportions of CB-ir interneurons in hominoids. Our data also show that, within individuals, areas V1 and V2 are distinguished from each other by a constant set of differences in interneuron distributions, suggesting that there are certain phylogenetically invariant transformations that reliably occur between these visual areas. Possible causes of interspecific variation in calcium-binding protein expression might include the influence of local neuronal activity [Patz et al., 2004] or species-specific changes in the distribution of transcription factors in the developing telencephalon that regulate GABAergic neurogenesis [Letinic et al., 2002; Xu et al., 2004]. These results show that phylogenetic variation exists in the inhibitory interneurons of visual cortex that might have consequences for sensory processing.

Acknowledgements

We thank E. Wahl, J. Hill, A. Zigo, A. Wolters, and K. Lever for technical assistance. We thank Drs. J.M. Erwin for helpful discussions and D.E. Wildman for phylogenetic data. This work was supported by the National Science Foundation (BCS-0515484, BCS-0549117, BCS-0453005, and IGERT-9987590), the Wenner-Gren Foundation for Anthropological Research, the James S. McDonnell Foundation (21002093 to T.M.P. and 22002078 to P.R.H.), Kent State University, the Center for Behavior Neuroscience (STC Program of the National Science Foundation, IBN-9876754) and the Yerkes National Primate Center (base grant from NCCR RR00165). Brain material used in this study was loaned by the Great Ape Aging Project, the Foundation for Comparative and Conservation Biology, the Cleveland Metroparks Zoo, the New England Primate Research Center, and the Kathleen Price Bryan Brain Bank at Duke University Hospital funded by NIA AG05128.

References

- Allman JM, Kaas JH (1971) Representation of the visual field in striate and adjoining cortex of the owl monkey (*Aotus trivirgatus*). *Brain Res* 35:89–106.
- Allman JM, McGuinness E (1988) Visual cortex in primates. In: *Comparative Primate Biology, Neurosciences* (Steklis H, Erwin J, ed), pp 279–326. New York: Alan R. Liss.
- Andressen C, Blümcke I, Celio MR (1993) Calcium-binding proteins: selective markers of nerve cells. *Cell Tissue Res* 271:181–208.
- Ballesteros-Yanez I, Munoz A, Contreras J, Gonzalez J, Rodriguez-Veiga E, DeFelipe J (2005) Double bouquet cell in the human cerebral cortex and a comparison with other mammals. *J Comp Neurol* 486:344–360.
- Boynton GM, Hegde J (2004) Visual cortex: the continuing puzzle of area V2. *Curr Biol* 14: R523–524.
- Brodman K (1909) *Vergleichende Lokalisationslehre der Großhirnrinde*. Leipzig: Barth.
- Carder RK, Leclerc SS, Hendry SH (1996) Regulation of calcium-binding protein immunoreactivity in GABA neurons of macaque primary visual cortex. *Cereb Cortex* 6:271–287.
- Changizi MA (2001) Principles underlying mammalian neocortical scaling. *Biol Cybern* 84:207–215.
- DeFelipe J (1997) Types of neurons, synaptic connections and chemical characteristics of cells immunoreactive for calbindin-D28k, parvalbumin and calretinin in the neocortex. *J Chem Neuroanat* 14:1–19.
- DeFelipe J, Alonso-Nanclares L, Arellano JJ (2002) Microstructure of the neocortex: comparative aspects. *J Neurocytol* 31:299–316.
- DeFelipe J, Gonzalez-Albo MC, del Rio MR, Elston GN (1999) Distribution and patterns of connectivity of interneurons containing calbindin, calretinin, and parvalbumin in visual areas of the occipital and temporal lobes of the macaque monkey. *J Comp Neurol* 412:515–526.
- DeFelipe J, Hendry SH, Jones EG (1989) Synapses of double bouquet cells in monkey cerebral cortex visualized by calbindin immunoreactivity. *Brain Res* 503:49–54.
- del Rio MR, DeFelipe J (1996) Colocalization of calbindin D-28k, calretinin, and GABA immunoreactivities in neurons of the human temporal cortex. *J Comp Neurol* 369:472–482.
- del Rio MR, DeFelipe J (1997a) Colocalization of parvalbumin and calbindin D-28k in neurons including chandelier cells of the human temporal neocortex. *J Chem Neuroanat* 12: 165–173.
- del Rio MR, DeFelipe J (1997b) Double bouquet cell axons in the human temporal neocortex: relationship to bundles of myelinated axons and colocalization of calretinin and calbindin D-28k immunoreactivities. *J Chem Neuroanat* 13:243–251.
- Dorph-Petersen KA, Nyengaard JR, Gundersen HJ (2001) Tissue shrinkage and unbiased stereological estimation of particle number and size. *J Microsc* 204:232–246.
- Douglas R, Martin KAC (1992) Exploring cortical microcircuits: A combined anatomical, physiological, and computational approach. In: *Single Neuron Computation* (McKenna T, Davies J, Zornetzer SF, eds), pp 381–412. San Diego, CA: Academic Press.
- Elston GN (2003) Pyramidal cell heterogeneity in the visual cortex of the nocturnal New World owl monkey (*Aotus trivirgatus*). *Neuroscience* 117:213–219.
- Elston GN, Rosa MG (1997) The occipitoparietal pathway of the macaque monkey: comparison of pyramidal cell morphology in layer III of functionally related cortical visual areas. *Cereb Cortex* 7:432–452.
- Elston GN, Benavides-Piccione R, Elston A, Zietsch B, Defelipe J, Manger P, Casagrande V, Kaas JH (2006) Specializations of the granular prefrontal cortex of primates: Implications for cognitive processing. *Anat Rec* 288A:26–35.
- Elston GN, Elston A, Kaas JH, Casagrande V (2005) Regional specialization in pyramidal cell structure in the visual cortex of the galago: an intracellular injection study of striate and extrastriate areas with comparative notes on New World and Old World monkeys. *Brain Behav Evol* 66:10–21.
- Elston GN, Rosa MG, Calford MB (1996) Comparison of dendritic fields of layer III pyramidal neurons in striate and extrastriate visual areas of the marmoset: a Lucifer yellow intracellular injection. *Cereb Cortex* 6:807–813.
- Felleman DJ, Van Essen DC (1991) Distributed hierarchical processing in the primate cerebral cortex. *Cereb Cortex* 1:1–47.
- Felsenstein J (1985) Phylogenies and the comparative method. *Am Nat* 125:1–15.
- Gabbott PL, Bacon SJ (1996) Local circuit neurons in the medial prefrontal cortex (areas 24a, b, c, 25 and 32) in the monkey: II. Quantitative areal and laminar distributions. *J Comp Neurol* 364:609–636.
- Gabbott PL, Dickie BG, Vaid RR, Headlam AJ, Bacon SJ (1997a) Local-circuit neurones in the medial prefrontal cortex (areas 25, 32 and 24b) in the rat: morphology and quantitative distribution. *J Comp Neurol* 377:465–499.
- Gabbott PL, Jays PR, Bacon SJ (1997b) Calretinin neurons in human medial prefrontal cortex (areas 24a, b, c, 32', and 25). *J Comp Neurol* 381:389–410.
- Garland T, Ives AR (2000) Using the past to predict the present: Confidence intervals for regression equations in phylogenetic comparative methods. *Am Nat* 155:346–364.
- Garland T, Harvey PH, Ives AR (1992) Procedures for the analysis of comparative data using phylogenetically independent contrasts. *Syst Biol* 41:18–32.
- Garland T, Midford PE, Ives AR (1999) An introduction to phylogenetically based statistical methods, with a new method for confidence intervals on ancestral values. *Am Zool* 39: 374–388.
- Glezer, II, Hof PR, Leranath C, Morgane PJ (1993) Calcium-binding protein-containing neuronal populations in mammalian visual cortex: a comparative study in whales, insectivores, bats, rodents, and primates. *Cereb Cortex* 3:249–272.
- Gonchar Y, Burkhalter A (1997) Three distinct families of GABAergic neurons in rat visual cortex. *Cereb Cortex* 7:347–358.
- Goodman M, Grossman LI, Wildman DE (2005) Moving primate genomics beyond the chimpanzee genome. *Trends Genet* 21:511–517.
- Gundersen HJ (1988) The nucleator. *J Microsc* 151:3–21.
- Harvey PH, Krebs JR (1990) Comparing brains. *Science* 249:140–146.
- Hässler R (1967) Comparative anatomy in the central visual systems in day- and night-active primates. In: *Evolution of the Forebrain* (Hässler R, Stephan H, eds), pp 419–434. Stuttgart: Thieme.
- Hendry SH, Carder RK (1993) Neurochemical compartmentation of monkey and human visual cortex: similarities and variations in calbindin immunoreactivity across species. *Vis Neurosci* 10:1109–1120.
- Hendry SHC, Jones EG, Emson PC, Lowson DEM, Heizmann CW, Streit P (1989) Two classes of cortical GABA neurons defined by differential calcium binding protein immunoreactivities. *Exp Brain Res* 76:467–472.
- Hof PR, Morrison JH (1995) Neurofilament protein defines regional patterns of cortical organization in the macaque monkey visual system: a quantitative immunohistochemical analysis. *J Comp Neurol* 352:161–186.
- Hof PR, Sherwood CC (2005) Morphomolecular neuronal phenotypes in the neocortex reflect phylogenetic relationships among certain mammalian orders. *Anat Rec* 287A:1153–1163.
- Hof PR, Glezer, II, Condé F, Flagg RA, Rubin MB, Nimchinsky EA, Vogt Weisenhorn DM (1999) Cellular distribution of the calcium-binding proteins parvalbumin, calbindin, and calretinin in the neocortex of mammals: phylogenetic and developmental patterns. *J Chem Neuroanat* 16:77–116.
- Howard CV, Reed MG (1998) *Unbiased Stereology – Three-Dimensional Measurement in Microscopy*. New York: Springer-Verlag.
- Hutsler JJ, Lee DG, Porter KK (2005) Comparative analysis of cortical layering and supragranular layer enlargement in rodent carnivore and primate species. *Brain Res* 1052: 71–81.

- Kaas JH (2005) The future of mapping sensory cortex in primates: three of many remaining issues. *Phil Trans R Soc Lond B Biol Sci* 360: 653–664.
- Kondo H, Hashikawa T, Tanaka K, Jones EG (1994) Neurochemical gradient along the monkey occipito-temporal cortical pathway. *Neuroreport* 5:613–616.
- Kondo H, Tanaka K, Hashikawa T, Jones EG (1999) Neurochemical gradients along monkey sensory cortical pathways: calbindin-immunoreactive pyramidal neurons in layers II and III. *Eur J Neurosci* 11:4197–4203.
- Kubota Y, Jones EG (1993) Co-localization of two calcium binding proteins in GABA cells of rat piriform cortex. *Brain Res* 600:339–344.
- Lee TS (2003) Computations in the early visual cortex. *J Physiol Paris* 97:121–139.
- Letinic K, Zoncu R, Rakic P (2002) Origin of GABAergic neurons in the human neocortex. *Nature* 417:645–649.
- Leuba G, Saini K (1997) Colocalization of parvalbumin, calretinin and calbindin D-28k in human cortical and subcortical visual structures. *J Chem Neuroanat* 13:41–52.
- Li CX, Callaway JC, Waters RS (2002) Removal of GABAergic inhibition alters subthreshold input in neurons in forepaw barrel subfield (FBS) in rat first somatosensory cortex (SI) after digit stimulation. *Exp Brain Res* 145: 411–428.
- Lund JS, Lewis DA (1993) Local circuit neurons of developing and mature macaque prefrontal cortex: Golgi and immunocytochemical characteristics. *J Comp Neurol* 328:282–312.
- Lund JS, Yoshioka T, Levitt JB (1993) Comparison of intrinsic connectivity in different areas of macaque monkey cerebral cortex. *Cereb Cortex* 3:148–162.
- Markram H, Toledo-Rodriguez M, Wang Y, Gupta A, Silberberg G, Wu C (2004) Interneurons of the neocortical inhibitory system. *Nat Rev Neurosci* 5:793–807.
- Morrison JH, Hof PR, Huntley GW (1998) Neurochemical organization of the primate visual cortex. In: *Handbook of Chemical Neuroanatomy* (Bloom FE, Björklund A, Hökfelt T, eds), pp 299–430. Amsterdam: Elsevier.
- Mountcastle VB (1997) The columnar organization of the neocortex. *Brain* 120:701–722.
- Mouton PR (2002) *Principles and Practices of Unbiased Stereology: An Introduction for Bioscientists*. Baltimore, MD: The Johns Hopkins University Press.
- Nunn CL, Barton RA (2001) Comparative methods for studying primate adaptation and allometry. *Evol Anthropol* 10:81–98.
- Pagel MD (1992) A method for the analysis of comparative data. *J Theor Biol* 156:431–442.
- Patz S, Grabert J, Gorba T, Wirth MJ, Wahle P (2004) Parvalbumin expression in visual cortical interneurons depends on neuronal activity and TrkB ligands during an early period of postnatal development. *Cereb Cortex* 14:342–351.
- Peterson DA, Dickinson-Anson HA, Leppert JT, Lee KF, Gage FH (1999) Central neuronal loss and behavioral impairment in mice lacking neurotrophin receptor p75. *J Comp Neurol* 404:1–20.
- Preuss TM (2000) Taking the measure of diversity: comparative alternatives to the model-animal paradigm in cortical neuroscience. *Brain Behav Evol* 55:287–299.
- Preuss TM, Coleman GQ (2002) Human-specific organization of primary visual cortex: alternating compartments of dense Cat-301 and calbindin immunoreactivity in layer 4A. *Cereb Cortex* 12:671–691.
- Preuss TM, Kaas JH (1996) Cytochrome oxidase ‘blobs’ and other characteristics of primary visual cortex in a lemuroid primate, *Cheirogaleus medius*. *Brain Behav Evol* 47:103–112.
- Preuss TM, Qi H, Kaas JH (1999) Distinctive compartmental organization of human primary visual cortex. *Proc Natl Acad Sci USA* 96:11601–11606.
- Price T (1997) Correlated evolution and independent contrasts. *Phil Trans R Soc Lond B Biol Sci* 352:519–529.
- Prothero J (1997) Scaling of cortical neuron density and white matter volume in mammals. *J Hirnforsch* 38:513–524.
- Purvis A, Webster AJ (1999) Phylogenetically independent comparisons and primate phylogeny. In: *Comparative Primate Socioecology* (Lee PC, ed), pp 44–68. Cambridge, UK: Cambridge University Press.
- Rilling JK, Insel TR (1999) The primate neocortex in comparative perspective using magnetic resonance imaging. *J Hum Evol* 37:191–223.
- Rockel AJ, Hiorns RW, Powell TPS (1980) The basic uniformity in structure of the neocortex. *Brain* 103:221–244.
- Rosa MG, Krubitzer LA (1999) The evolution of visual cortex: where is V2? *Trends Neurosci* 22:242–248.
- Rosa MG, Fritsches KA, Elston GN (1997) The second visual area in the marmoset monkey: visuotopic organisation, magnification factors, architectonical boundaries, and modularity. *J Comp Neurol* 387:547–567.
- Rosa MG, Palmer SM, Gamberini M, Tweedale R, Pinon MC, Bourne JA (2005) Resolving the organization of the New World monkey third visual complex: the dorsal extrastriate cortex of the marmoset (*Callithrix jacchus*). *J Comp Neurol* 483:164–191.
- Sato H, Katsuyama N, Tamura H, Hata Y, Tsutomoto T (1995) Mechanisms underlying direction selectivity of neurons in the primary visual cortex of the macaque. *J Neurophysiol* 74:1382–1394.
- Schmitz C, Hof PR (2000) Recommendations for straightforward and rigorous methods of counting neurons based on a computer simulation approach. *J Chem Neuroanat* 20:93–114.
- Semendeferi K, Armstrong E, Schleicher A, Zilles K, Van Hoesen GW (1998) Limbic frontal cortex in hominoids: a comparative study of area 13. *Am J Phys Anthropol* 106: 129–155.
- Semendeferi K, Armstrong E, Schleicher A, Zilles K, Van Hoesen GW (2001) Prefrontal cortex in humans and apes: a comparative study of area 10. *Am J Phys Anthropol* 114: 224–241.
- Sherwood CC, Hof PR (in press) The evolution of neuron types and cortical histology in apes and humans. In: *The Evolution of Primate Nervous Systems. Evolution of Nervous Systems, Vol. 4* (Preuss TM, Kaas JH, eds), Amsterdam: Elsevier.
- Sherwood CC, Holloway RL, Erwin JM, Hof PR (2004) Cortical orofacial motor representation in Old World monkeys, great apes, and humans. II. Stereologic analysis of chemoarchitecture. *Brain Behav Evol* 63:82–106.
- Sherwood CC, Lee PWH, Rivara C-B, Holloway RL, Gilissen EPE, Simmons RMT, Hakeem A, Allman JM, Erwin JM, Hof PR (2003) Evolution of specialized pyramidal neurons in primate visual and motor cortex. *Brain Behav Evol* 61:28–44.
- Sincich LC, Horton JC (2005) The circuitry of V1 and V2: integration of color, form, and motion. *Annu Rev Neurosci* 28:303–326.
- Sokal RR, Rohlf FJ (1995) *Biometry: The Principles and Practice of Statistics in Biological Research*. San Francisco, CA: W.H. Freeman.
- Somogyi P, Tamas G, Lujan R, Buhl EH (1998) Salient features of synaptic organisation in the cerebral cortex. *Brain Res Rev* 26:113–135.
- Stephan H, Frahm HD, Baron G (1981) New and revised data on volumes of brain structures in insectivores and primates. *Folia Primatol* 35:1–29.
- Tosi AJ, Melnick DJ, Disotell TR (2004) Sex chromosome phylogenetics indicate a single transition to terrestriality in the guenons (tribe Cercopithecini). *J Hum Evol* 46:223–237.
- Tower DB (1954) Structural and functional organization of mammalian cerebral cortex: the correlation of neurone density with brain size. *J Comp Neurol* 101:19–52.
- Tower DB, Young OM (1973) The activities of butyrylcholinesterase and carbonic anhydrase, the rate of anaerobic glycolysis and the question of constant density of glial cells in cerebral cortices of mammalian species from mouse to whale. *J Neurochem* 20:269–278.
- Tsumoto T, Eckart W, Creutzfeldt OD (1979) Modification of orientation sensitivity of cat visual cortex neurons by removal of GABA-mediated inhibition. *Exp Brain Res* 34:351–363.

- Van Brederode JF, Mulligan KA, Hendrickson AE (1990) Calcium-binding proteins as markers for subpopulations of GABAergic neurons in monkey striate cortex. *J Comp Neurol* 298:1–22.
- Van Essen DC, Anderson CH, Felleman DJ (1992) Information processing in the primate visual system: an integrated systems perspective. *Science* 255:419–423.
- Wang J, Caspary D, Salvi RJ (2000a) GABA-A antagonist causes dramatic expansion of tuning in primary auditory cortex. *Neuroreport* 11:1137–1140.
- Wang Y, Fujita I, Murayama Y (2000b) Neuronal mechanisms of selectivity for object features revealed by blocking inhibition in inferotemporal cortex. *Nat Neurosci* 3: 807–813.
- Warton DI, Weber NC (2002) Common slope tests for bivariate structural relationships. *Biometrical J* 44:161–174.
- West MJ, Slomianka L, Gundersen HJG (1991) Unbiased stereological estimation of the total number of neurons in the subdivisions of the rat hippocampus using the optical fractionator. *Anat Rec* 231:482–497.
- Xu Q, Cobos I, De La Cruz E, Rubenstein JL, Anderson SA (2004) Origins of cortical interneuron subtypes. *J Neurosci* 24:2612–2622.
- Zilles K, Rehkämper G (1988) The brain, with special reference to the telencephalon. In: *Orang-utan Biology* (Schwartz JH, ed), pp 157–176. New York: Oxford University Press.
- Zilles K, Palomero-Gallagher N, Schleicher A (2004) Transmitter receptors and functional anatomy of the cerebral cortex. *J Anat* 205: 417–432.